

The dynamically generated h_1 state by the $K^*\bar{K}^*$ interaction and its $K_1(1270)\bar{K}$ and $b_1(1235)\pi$ decays

Qing-Hua Shen,^{1,2,3,*} Li-Sheng Geng,^{4,5,6,7,8,†} Xiang Liu,^{2,9,10,11,‡} and Ju-Jun Xie^{1,3,8,§}

¹*State Key Laboratory of Heavy Ion Science and Technology,*

Institute of Modern Physics, Chinese Academy of Sciences, Lanzhou 730000, China

²*School of Physical Science and Technology, Lanzhou University, Lanzhou 730000, China*

³*School of Nuclear Sciences and Technology, University of Chinese Academy of Sciences, Beijing 101408, China*

⁴*School of Physics, Beihang University, Beijing 102206, China*

⁵*Sino-French Carbon Neutrality Research Center, Ecole Centrale de Pekin/School*

of General Engineering, Beihang University, Beijing 100191, China

⁶*Peng Huanwu Collaborative Center for Research and Education,*

International Institute for Interdisciplinary and Frontiers, Beihang University, Beijing 100191, China

⁷*Beijing Key Laboratory of Advanced Nuclear Materials and Physics, Beihang University, Beijing 102206, China*

⁸*Southern Center for Nuclear-Science Theory (SCNT), Institute of Modern Physics,*

Chinese Academy of Sciences, Huizhou 516000, China

⁹*Lanzhou Center for Theoretical Physics, Key Laboratory of Theoretical Physics of Gansu Province,*

Key Laboratory of Quantum Theory and Applications of MoE,

Gansu Provincial Research Center for Basic Disciplines of Quantum Physics, Lanzhou University, Lanzhou 730000, China

¹⁰*MoE Frontiers Science Center for Rare Isotopes, Lanzhou University, Lanzhou 730000, China*

¹¹*Research Center for Hadron and CSR Physics, Lanzhou University & Institute of Modern Physics of CAS, Lanzhou 730000, China*

(■Dated: January 21, 2026)

We investigate the dynamically generated h_1 state with spin-parity $J^P = 1^+$ and a mass around 1790 MeV, arising from the $K^*\bar{K}^*$ interaction within the chiral unitary approach. The partial decay widths into the $K_1(1270)\bar{K}$ and $b_1(1235)\pi$ channels are calculated via a triangular loop mechanism. In this mechanism, the h_1 state couples to $K^*\bar{K}^*$, and final-state interactions between K^* and \bar{K}^* proceed through pseudoscalar-meson exchange, leading to the final states \bar{K} (or π) and $K_1(1270)$ [or $b_1(1235)$]. We also present the invariant mass distributions of a vector meson and a pseudoscalar meson originating from the decays of $K_1(1270)$ or $b_1(1235)$, along with the corresponding decay widths. Our results show that these decay widths are all of the order of a few MeV. We hope that future experiments can test the predictions presented here, thereby helping to identify this h_1 state.

I. INTRODUCTION

Hadron spectroscopy provides essential insights into the nonperturbative behavior of the strong interaction. Over the past decades, the field has advanced significantly, particularly with the observation of numerous new hadronic states such as the XYZ and P_c particles, which have attracted broad attention. A central goal of modern hadron spectroscopy is the identification of exotic configurations—including multiquark states, glueballs, and hybrids. These newly discovered states offer valuable opportunities to address this challenge.

In this context, the molecular picture has been widely employed to interpret and predict many of these hadrons, where exotic states are understood as bound systems of color-singlet hadrons (for reviews, see e.g., Refs. [1–12]). Theoretically, molecular states are often treated as dynamically generated resonances or bound states emerging from the interactions

among their constituent hadrons. A key approach in this direction is the chiral unitary theory (ChUT), which has become a useful tool in the field and has produced many important results (see, e.g., Refs. [13–41]).

In Ref. [26], an h_1 state is dynamically generated by the interaction between two vector mesons in the $K^*\bar{K}^*$ channel with strangeness=0, isospin=0, and spin=1. Moreover, the $K^*\bar{K}^*$ is the only one channel in this sector. According to the $K^*\bar{K}^*$ nature of this h_1 state, the near threshold enhancement in the $K^*\bar{K}^*$ mass distribution of the process $J/\psi \rightarrow \eta K^{*0}\bar{K}^{*0}$ measured by the BES Collaboration [42] was investigated with the contribution of the h_1 state [43], which provides further support for the existence of a h_1 state with mass around 1830 ± 20 MeV and width about 110 ± 10 MeV¹. Subsequently, Ref. [44] suggests that this h_1 state can be searched for via the process $\eta_c/\eta_c(2S) \rightarrow \phi K^*\bar{K}^*$ experimentally.

However, since the mass of this h_1 state lies very close to the $K^*\bar{K}^*$ mass threshold, its signal becomes strongly suppressed in the $K^*\bar{K}^*$ invariant mass spectrum. Moreover,

* shenqinghua@impcas.ac.cn

† lisheng.geng@buaa.edu.cn

‡ xiangliu@lzu.edu.cn

§ xiejujun@impcas.ac.cn

¹ In that reference, the mass and width of the h_1 state were evaluated from the module squared of the $K^*\bar{K}^* \rightarrow K^*\bar{K}^*$ scattering amplitude.

there are no accessible two-pseudoscalar-meson decay channels [43]. The pseudoscalar-vector channel is allowed, but these processes involve anomalous couplings, which are generally considered small due to the higher-order nature of the anomalous term in the chiral expansion [45]. It is therefore necessary to search for it in alternative decay channels. Along this line, we investigate in this work its decays into $K_1(1270)\bar{K}$ and $b_1(1235)\pi$ channels, where we consider $K_1(1270)$ and $b_1(1235)$ as dynamically generated by the interaction of vector and pseudoscalar mesons [18].

This article is organized as follows. In the next section, we present the h_1 state dynamically generated by the interaction of two vector mesons in the sector with strangeness=0, isospin=0, and spin=1, and discuss its dynamic generation. In Sect. III, we present the relevant theoretical formalism for the reaction mechanisms of $h_1 \rightarrow K_1(1270)\bar{K}$ and $h_1 \rightarrow b_1(1235)\pi$, and the numerical results and discussion are given. Finally, we give a summary in Sect. V.

II. AN h_1 STATE DYNAMICALLY GENERATED FROM THE $K^*\bar{K}^*$ INTERACTION

Following Ref. [26], the coupled-channel vector meson-vector meson scattering can be studied with the hidden gauge Lagrangians

$$\mathcal{L}_{VVVV} = \frac{1}{2}g^2\langle [V_\mu, V_\nu]V^\mu V^\nu \rangle, \quad (1)$$

$$\mathcal{L}_{VVV} = ig\langle (V^u \partial_\nu V_\mu - \partial_\nu V_\mu V^u) V^\nu \rangle, \quad (2)$$

where $g = \frac{M_V}{2f}$, with $M_V = M_\rho$, the mass of the ρ meson, and $f = 93$ MeV, the pion decay constant. The $\langle \rangle$ denotes the trace in flavor space. V_μ stands for the vector nonet, which is given by:

$$V_\mu = \begin{pmatrix} \frac{1}{\sqrt{2}}(\omega + \rho^0) & \rho^+ & K^{*+} \\ \rho^- & \frac{1}{\sqrt{2}}(\omega - \rho^0) & K^{*0} \\ K^{*0} & \bar{K}^{*0} & \phi \end{pmatrix}_\mu. \quad (3)$$

For the $K^*\bar{K}^*$ interaction, the domain mechanisms are shown in Fig. 1, where the four-vector-contact term [Fig. 1 (a)] and the $t(u)$ -channel vector meson exchange [Fig. 1 (b)] are included. Then, one can get the effective interaction vertex, which is shown in Fig. 1 (c).

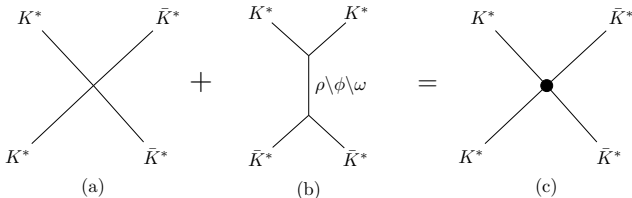


FIG. 1. The mechanisms of the $K^*\bar{K}^*$ meson interaction. (a): four-vector-contact term. (b): $t(u)$ -channel vector meson exchange. (c): the effective interaction vertex of $K^*\bar{K}^* \rightarrow K^*\bar{K}^*$ at tree level.

The tree-level $K^*\bar{K}^* \rightarrow K^*\bar{K}^*$ transition amplitude V in s -wave can be obtained as [26],

$$V = \frac{g^2[M_\rho^2 M_\phi^2 + (2M_\rho^2 + 3M_\phi^2)M_\omega^2](4M_{K^*}^2 - 3s)}{4M_\rho^2 M_\phi^2 M_\omega^2}, \quad (4)$$

where s is the invariant mass squared of the $K^*\bar{K}^*$ system, and M_V ($V = \rho, \omega, \phi$, and K^*) stands for the mass of the vector meson.

Then, we can obtain the unitarized T -matrix of the $K^*\bar{K}^* \rightarrow K^*\bar{K}^*$ scattering in the s -wave as follows,

$$T = (1 - V\tilde{G})^{-1}V, \quad (5)$$

where \tilde{G} is the convoluted loop function to take into account the width of the K^* meson [26, 43],

$$\tilde{G}(s) = \int_{m_-^2}^{m_+^2} dm_1^2 dm_2^2 A(m_1^2) A(m_2^2) G(s, m_1^2, m_2^2), \quad (6)$$

$$A(m^2) = \frac{1}{N} \text{Im} \frac{1}{m^2 - m_{K^*}^2 + i\Gamma(m^2)m}, \quad (7)$$

$$N = \int_{m_-^2}^{m_+^2} dm^2 \frac{1}{m^2 - m_{K^*}^2 + im\Gamma(m^2)}, \quad (8)$$

$$\Gamma(m^2) = \Gamma_{K^*} \frac{p^3(m^2)}{p^3(m_{K^*}^2)} \theta(m - m_K - m_\pi), \quad (9)$$

$$p(m^2) = \frac{\lambda(m^2, m_\pi^2, m_K^2)}{2m}, \quad (10)$$

where $m_+ = M_{K^*} + 2\Gamma_{K^*}$ and $m_- = M_{K^*} - 2\Gamma_{K^*}$ are the upper and lower limits of the integration, respectively. The loop function G is given by

$$G(s, m_1^2, m_2^2) = i \int \frac{d^4q}{(2\pi)^4} \frac{1}{s - m_1^2 + i\epsilon} \frac{1}{s - m_2^2 + i\epsilon}. \quad (11)$$

It is convenient to deal with it by the dimensional regularization method,

$$16\pi^2 G(s, m_1^2, m_2^2) = a(\mu) + \log \frac{m_1 m_2}{\mu^2} + \frac{\Delta}{2s} \log \frac{m_2^2}{m_1^2} + \frac{\nu}{2s} \left(\log \frac{s - \Delta + \nu}{-s + \Delta + \nu} + \log \frac{s + \Delta + \nu}{-s - \Delta + \nu} \right), \quad (12)$$

with $\Delta = m_2^2 - m_1^2$, $\nu = \lambda^{\frac{1}{2}}(s, m_1^2, m_2^2)$, and the Källen function $\lambda(x, y, z) = x^2 + y^2 + z^2 - 2xy - 2yz - 2xz$. In addition, μ is the scale of dimensional regularization, and changes in the scale are reabsorbed in the subtraction constant $a(\mu)$, so that the results remain scale independent. In this work, we take $\mu = 1000$ MeV, as used in previous works [26, 43].

With this formalism and the former ingredients, one can easily obtain the $K^*\bar{K}^* \rightarrow K^*\bar{K}^*$ scattering matrix T . Then, one can also look for poles of the scattering amplitude T on the complex plane of s . The pole, s_{pole} , on the second Riemann sheet could be associated with the h_1 state. The real part of $\sqrt{s_{\text{pole}}}$ is associated with the mass of the state, and the minus imaginary part of $\sqrt{s_{\text{pole}}}$ is associated with one-half of its width.

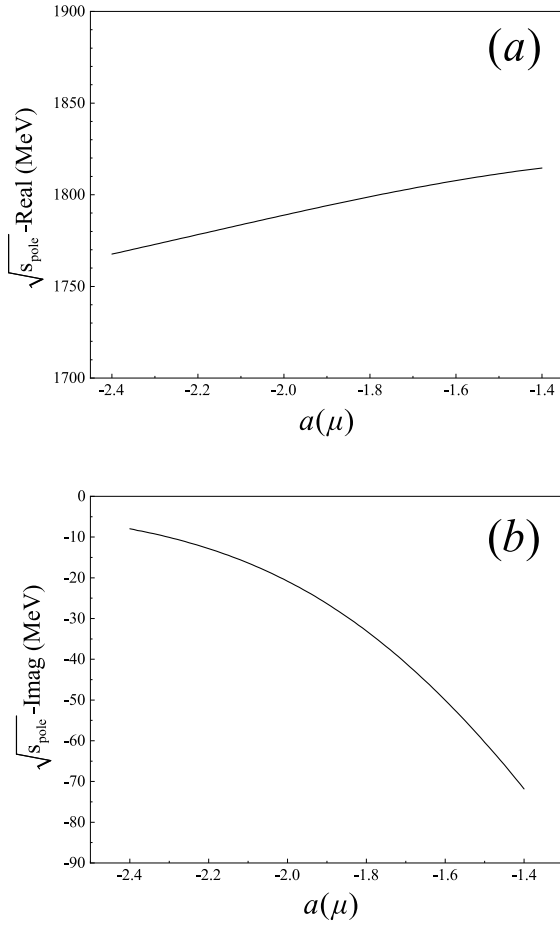


FIG. 2. The real (a) and imaginary (b) parts of the pole position of the $K^*\bar{K}^* \rightarrow K^*\bar{K}^*$ scattering amplitude as a function of the subtraction constant $a(\mu)$.

In Fig. 2, we show the real and imaginary parts of the pole position of the h_1 state as a function of the subtraction constant $a(\mu)$. With the increase of the subtraction constant $a(\mu)$, the mass of h_1 becomes larger, and its width becomes broader. Note that, after including the width of K^* and \bar{K}^* , in the range of -2.4 to -1.4 for $a(\mu)$, one can always find a pole for the h_1 state with a mass $M_{h_1} = 1790 \pm 25$ MeV, while its width changes much.

Close to the pole position, s_{pole} , the scattering amplitude T can be parameterized as the spin projection operator, which projects the vector meson-vector meson pair $K^*\bar{K}^*$ into spin 1 with

$$T = \mathcal{P}^{(1)}(K^*\bar{K}^*) \frac{|g_{h_1 K^* \bar{K}^*}|^2}{s - s_{\text{pole}}} \mathcal{P}^{(1)}(K^*\bar{K}^*), \quad (13)$$

where $g_{h_1 K^* \bar{K}^*}$ is the strong coupling constant of the dynamically generated h_1 state to the $K^*\bar{K}^*$ channel. And $\mathcal{P}^{(1)}$ is written as

$$\mathcal{P}^{(1)}(K^*\bar{K}^*) = \frac{1}{2} [\epsilon_i(K^*)\epsilon_j(\bar{K}^*) - \epsilon_j(K^*)\epsilon_i(\bar{K}^*)]. \quad (14)$$

Thus, by determining the residues of the scattering amplitude

T at the pole position, one can obtain the coupling constant $g_{h_1 K^* \bar{K}^*}$, which is complex in general.

In Fig. 3, we show the theoretical results of $g_{h_1 K^* \bar{K}^*}$ (in units of GeV) as a function of $a(\mu)$. It is found that the imaginary part of $g_{h_1 K^* \bar{K}^*}$ is small compared with its real part.

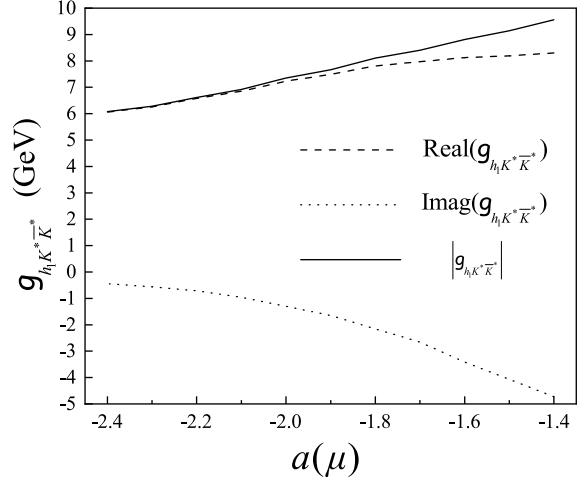


FIG. 3. Coupling constant of the dynamically generated h_1 state to the $K^*\bar{K}^*$ channel as a function of the subtraction constant $a(\mu)$.

III. THE $h_1 \rightarrow K_1(1270)\bar{K} \rightarrow K^{*+}\pi^0K^-$ AND $h_1 \rightarrow b_1(1235)\pi \rightarrow \omega(\phi)\pi^+\pi^-$ DECAYS

In this section, we study the $h_1 \rightarrow \bar{K}K_1(1270)$ and $\pi b_1(1235)$ decays within a triangular loop mechanism, where the h_1 state couples to the $K^*\bar{K}^*$ channel, and then the final-state interactions between K^* and \bar{K}^* transition to a \bar{K} (or π) and $K_1(1270)$ [or $b_1(1235)$] through the exchange of pseudo-scalar mesons. Here, the axial-vector mesons $K_1(1270)$ and $b_1(1235)$ are viewed as dynamically generated from the vector meson-pseudo-scalar meson interactions in coupled channels [18]. Thus, the produced $K_1(1270)$ and $b_1(1235)$ resonances then decay into a vector meson plus a pseudo-scalar meson. This decay mechanism is illustrated in Fig. 4, where V_f , P_1 , and P_2 stand for vector mesons and pseudo-scalar mesons in the final state.

For the $K_1(1270)$ state, it has a two-pole structure in the dynamical generation picture [18, 22, 46, 47]. One state corresponds to the lower pole around $(1195 - i123)$ MeV, which is referred to as " $K_{1L}(1270)$ ", while the other one around 1280 MeV is called $K_{1H}(1270)$. The lower one, $K_{1L}(1270)$, mainly couples to the $K^*\pi$ channel. For the $K_{1H}(1270)$, it mainly couples to the $K^*\eta$ channel. Here, we only consider the $K_{1L}(1270)$ state, since the $h_1 \rightarrow \bar{K}K_{1H}(1270)$ is suppressed due to the phase space. For the $b_1(1235)$ state, its pole position is $(1247 - i28)$ MeV, and it can decay into $\omega\pi$ and $\phi\pi$ channels.

To compute the decay amplitudes of the processes shown in Fig. 4, we also need the AVP and VPP interactions, where

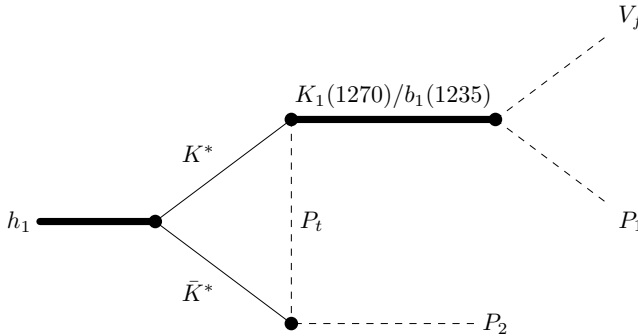


FIG. 4. Diagrammatic representation of the triangular loop mechanism for the $h_1 \rightarrow K_1(1270)/b_1(1235)P_2 \rightarrow V_f P_1 P_2$ decay. V_f , P_1 and P_2 stand for the vector meson and pseudoscalar mesons in the final state.

A , V , and P stand for axial-vector, vector, and pseudo-scalar mesons, respectively. In this work, the effective interaction for the VPP vertex is written as [25, 26]

$$\mathcal{L}_{VPP} = -ig \langle V_\mu [P, \partial^\mu P] \rangle. \quad (15)$$

For the AVP vertex, the effective interactions can be written as [48–52]

$$t_{AVP} = g_{AVP} \epsilon_A \cdot \epsilon_V, \quad (16)$$

where ϵ_A and ϵ_V are the polarization four-vectors of the axial-vector and vector mesons, respectively. Their explicit forms can be found in Refs [53, 54]. The coupling constant g_{AVP} can be determined around the pole position of the dynamically generated axial-vector state as discussed before for the case of $g_{h_1 K^* \bar{K}^*}$. We show those involved coupling constants in this work in Table I, which are similar to those obtained in Refs. [18, 22].

TABLE I. The coupling constants (in units of MeV) of the $K_{1L}(1270)$ and $b_1(1235)$ mesons for different channels.

$K_{1L}(1270)$	
$K^* \eta$	$72 + i197$
$K^* \pi$	$4747 - i2874$
$b_1(1235)$	
$\frac{1}{\sqrt{2}}(\bar{K}^* K + K^* \bar{K})$	$6172 - i75$
$\phi \pi$	$2087 - i385$
$\omega \pi$	$-1869 + i300$

With the formalism and ingredients outlined above, we can write down the decay amplitude for $h_1 \rightarrow AP_1 \rightarrow V_f P_1 P_2$

depicted in Fig. 4 as

$$t = C g g_{h_1 K^* \bar{K}^*} g_{AV_1 P_t} g_{AV_f P_1} \int \frac{d^4 q}{(2\pi)^4} \quad (17)$$

$$\times \frac{t_a F^2}{q^2 - m_{K^*}^2 + im_{K^*} \Gamma_{K^*}} \times \frac{1}{(P - q)^2 - m_{K^*}^2 + im_{K^*} \Gamma_{K^*}} \quad (18)$$

$$\times \frac{1}{(q - k_A)^2 - m_{P_t}^2 + i\epsilon}, \quad (19)$$

with

$$t_a = i \sum_{V_A} \mathcal{P}^{(1)*}(K^* \bar{K}^*) \epsilon^*(k_A) \cdot \epsilon(q) \times \frac{(k_{P_2} + q - k_A) \cdot \epsilon(P - q) \epsilon(k_A) \cdot \epsilon^*(k_{V_f})}{k_A^2 - m_A^2 + im_A \Gamma_A}, \quad (20)$$

where P , k_A , k_{V_f} , k_{P_1} , and k_{P_2} are the four-momenta of the decay state h_1 , axial-vector A [$\equiv K_1(1270)$ or $b_1(1235)$], final vector mesons V_f , pseudo-scalar mesons P_1 and P_2 , respectively. The q represents the free momentum in the triangular loop. k_{V_f} can be obtained by transforming k'_{V_f} from the rest frame of V_f and P_1 to the center-of-mass frame of the initial h_1 state using Lorentz transformation. In this frame, $k'_{V_f} = (E'_{V_f}, |\vec{k}'_{V_f}| \sin\alpha \cos\beta, |\vec{k}'_{V_f}| \sin\alpha \sin\beta, |\vec{k}'_{V_f}| \cos\alpha)$, where α and β are the polar and azimuth angles, respectively. The energy E'_{V_f} and momentum $|\vec{k}'_{V_f}|$ is obtained in the center-of-mass frame of the decaying particle A as

$$E'_{V_f} = \frac{m_A^2 + m_{V_f}^2 - m_{P_1}^2}{2M_A}, \quad |\vec{k}'_{V_f}| = \sqrt{E'^2_{V_f} - m_{V_f}^2}. \quad (21)$$

To account for the off-shell effects of the exchanged pseudoscalar meson, a form factor F is introduced [25, 26, 55–58].

$$F = \frac{\Lambda_t^2 - m_{P_t}^2}{\Lambda_t^2 - (E_A - M_{h_1}/2)^2 + |\vec{q} - \vec{k}_A|^2}, \quad (22)$$

$$E_A = \frac{M_{h_1}^2 + m_A^2 - m_{P_2}^2}{2M_{h_1}}, \quad (23)$$

$$|\vec{k}_A| = \sqrt{E_A^2 - m_A^2}, \quad (24)$$

where M_{h_1} is the mass of the dynamically generated h_1 meson, and E_A is the energy of dynamically generated low axial-vector meson A . A cut-off parameter Λ_t is also included, and we will discuss it later.

The coefficient C in Eq. (19) is an isospin factor, which can

be obtained with the following relations [59–61]:

$$\begin{aligned} |K^* \bar{K}^*\rangle_{(0,0)} &= -\frac{1}{\sqrt{2}}(|K^{*+}K^{*-}\rangle + |K^{*0}\bar{K}^{*0}\rangle), \\ |K^* \bar{K} + cc.\rangle_{(1,0)} &= \frac{1}{2}\left(|\bar{K}^{*0}K^0\rangle - |K^{*-}K^-\rangle\right. \\ &\quad \left.- |K^{*+}K^-\rangle + |K^{*0}\bar{K}^0\rangle\right), \end{aligned} \quad (26)$$

$$|K^* \bar{K} + cc.\rangle_{(1,-1)} = -\frac{1}{\sqrt{2}}(|K^{*-}K^0\rangle + |K^{*0}K^-\rangle), \quad (27)$$

$$|K^* \bar{K} + cc.\rangle_{(1,1)} = \frac{1}{\sqrt{2}}(|K^{*0}K^+\rangle + |K^{*0}K^{*+}\rangle), \quad (28)$$

$$|K^* \pi\rangle_{(\frac{1}{2}, -\frac{1}{2})} = \frac{1}{\sqrt{3}}|K^{*0}\pi^0\rangle - \sqrt{\frac{2}{3}}|K^{*+}\pi^-\rangle, \quad (29)$$

$$|K^* \pi\rangle_{(\frac{1}{2}, \frac{1}{2})} = -\sqrt{\frac{2}{3}}|K^{*0}\pi^+\rangle - \frac{1}{\sqrt{3}}|K^{*+}\pi^0\rangle, \quad (30)$$

$$|K^* \eta\rangle_{(\frac{1}{2}, \frac{1}{2})} = |K^{*+}\eta\rangle, \quad (31)$$

$$|K^* \eta\rangle_{(\frac{1}{2}, -\frac{1}{2})} = |K^{*0}\eta\rangle, \quad (32)$$

$$|\omega \pi\rangle_{(1,1)} = |\omega \pi^+\rangle, \quad |\omega \pi\rangle_{(1,0)} = |\omega \pi^0\rangle, \quad (33)$$

$$|\omega \pi\rangle_{(1,-1)} = |\omega \pi^-\rangle, \quad (34)$$

$$|\phi \pi\rangle_{(1,1)} = |\phi \pi^+\rangle, \quad |\phi \pi\rangle_{(1,0)} = |\phi \pi^0\rangle, \quad (35)$$

$$|\phi \pi\rangle_{(1,-1)} = |\phi \pi^-\rangle, \quad (36)$$

where (\cdot, \cdot) presents (I, I_z) with I and I_z are the total isospin and its third component.

The obtained values of the factor C are shown in Table II. The corresponding decay processes of $h_1 \rightarrow K_1^+(1270)K^- \rightarrow K^{*+}\pi^0K^-$ and $h_1 \rightarrow b_1^+(1235)\pi^- \rightarrow \omega(\phi)\pi^+\pi^-$ are presented in Figs. 5 and 6, respectively.

TABLE II. Coefficients C for $h_1 \rightarrow AP_2 \rightarrow V_f P_1 P_2$ decays.

$h_1 \rightarrow K_1^+(1270)K^- \rightarrow K^{*+}\pi^0K^-$						
P_t	A	V_f	P_1	P_2	C	
K^{*+}	K^{*-}	η	$K_1^+(1270)$	K^{*+}	π^0	K^-
K^{*+}	K^{*-}	π^0	$K_1^+(1270)$	K^{*+}	π^0	K^-
K^{*0}	\bar{K}^{*0}	π^-	$K_1^+(1270)$	K^{*+}	π^0	K^-
$h_1 \rightarrow b_1^+(1235)\pi^- \rightarrow \omega\pi^+\pi^-$						
K^{*+}	K^{*-}	K^0	$b_1^+(1235)$	ω	π^+	π^-
\bar{K}^{*0}	K^{*0}	K^-	$b_1^+(1235)$	ω	π^+	π^-
$h_1 \rightarrow b_1^+(1235)\pi^- \rightarrow \phi\pi^+\pi^-$						
K^{*+}	K^{*-}	K^0	$b_1^+(1235)$	ϕ	π^+	π^-
\bar{K}^{*0}	K^{*0}	K^-	$b_1^+(1235)$	ϕ	π^+	π^-

Then, we can obtain the invariant mass distribution of V_f and P_1 for the $h_1 \rightarrow AP_2 \rightarrow V_f P_1 P_2$ decay as,

$$\frac{d\Gamma_{h_1 \rightarrow AP_2 \rightarrow V_f P_1 P_2}}{dM_{V_f P_1}} = \int_{\Omega} \frac{d\Omega}{(2\pi)^4} \frac{|\vec{k}_A||\vec{k}'_{V_f}|}{8M_{h_1}^2} \frac{1}{3} \sum_{pol} |t|^2, \quad (37)$$

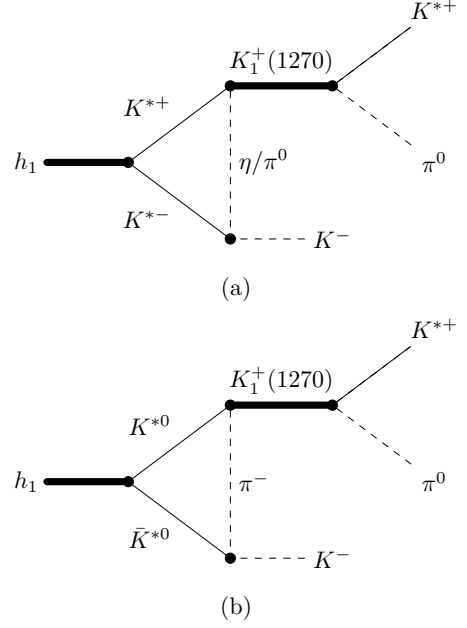


FIG. 5. Diagrammatic representation of the decay mechanisms $h_1 \rightarrow K_1^+(1270)K^- \rightarrow K^{*+}\pi^0K^-$ through the $K^*-\bar{K}^*-\pi/\eta$ triangle loop.

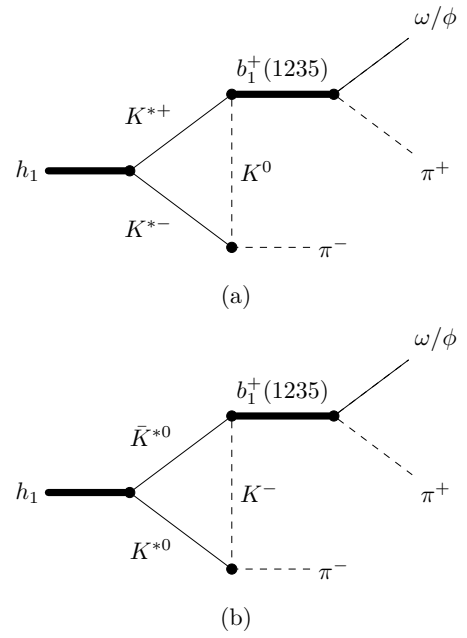


FIG. 6. Diagrammatic representation of the decay mechanisms $h_1 \rightarrow b_1^+(1235)\pi^- \rightarrow \omega(\phi)\pi^+\pi^-$ through the $K^*-\bar{K}^*-K$ triangle loop.

where we sum and average the spin polarizations of h_1 and V_f . Here, Ω is the solid angle in the rest frame of V_f and P_1 , and the differential solid angle is given by $d\Omega = \sin\alpha d\alpha d\beta$. The partial decay width of $h_1 \rightarrow AP_2 \rightarrow V_f P_1 P_2$ can be also

obtained by [62]

$$\Gamma_{h_1 \rightarrow AP_2 \rightarrow V_f P_1 P_2} = \int_{m_A - 2\Gamma_A}^{m_A + 2\Gamma_A} dM_{V_f P_1} \times \frac{d\Gamma_{h_1 \rightarrow AP_2 \rightarrow V_f P_1 P_2}}{dM_{V_f P_1}}, \quad (38)$$

where m_A and Γ_A are the mass and width of the dynamically generated axial-vector A mesons, respectively. Here, we take $m_{K_1(1270)} = 1195$ MeV, $\Gamma_{K_1(1270)} = 246$ MeV, $m_{b_1(1235)} = 1247$ MeV, and $\Gamma_{b_1(1235)} = 56$ MeV.

To calculate the decay amplitude t in Eq. (19), we first integrate over the q^0 by the residue theorem, then deal with $|\vec{q}|$ by the cutoff method in the spherical coordinates, where $\Lambda = \Lambda_t = 1350 \pm 100$ MeV is used, which is obtained by matching the experimental data of the two-pseudoscalar-meson decay modes for the dynamically generated scalar and tensor states of two vector mesons [53].

Besides, in the calculations, we take

$$\begin{aligned} q &= (q^0, |\vec{q}| \sin\theta \cos\phi, |\vec{q}| \sin\theta \sin\phi, |\vec{q}| \cos\theta), \\ k_A &= (E_A, |\vec{k}_A|, 0, 0), \\ k_{P_2} &= (M_{h_1} - E_A, -|\vec{k}_A|, 0, 0). \end{aligned} \quad (39)$$

IV. NUMERICAL RESULTS AND DISCUSSIONS

In Fig. 7, we first show the invariant mass distribution of $K^{*+}\pi^0$ for $h_1 \rightarrow K_1^+(1270)K^- \rightarrow K^{*+}\pi^0K^-$ process [Fig. 7(a)], $\omega\pi^+$ for $h_1 \rightarrow b_1^+(1235)\pi^- \rightarrow b_1^+(1235) \rightarrow \omega\pi^+\pi^-$ process [Fig. 7(b)], and $\phi\pi^+$ for $h_1 \rightarrow b_1^+(1235)\pi^- \rightarrow \phi\pi^+\pi^-$ process [Fig. 7(c)] with $a(\mu) = -1.7$ (solid line), -2.0 (dashed line), and -2.3 (dotted line), respectively, where the cutoff $\Lambda_t = 1350$ MeV. Note that with different values of $a(\mu)$, the mass of the h_1 resonance is also different. For the different cutoffs Λ_t , the line shapes of these invariant mass distributions are similar.

In Fig. 7 (a), one can see that the bump structure for the $K_{1L}(1270)$ resonance is lower than the value of the real part of its pole position, which is 1195 MeV. This is because the mass threshold of $K_{1L}(1270)\bar{K}$ is close to the mass of h_1 , and the width of $K_{1L}(1270)$ is relatively large. The available phase space for the $h_1 \rightarrow K_{1L}(1270)K^- \rightarrow K^{*0}\pi^+K^-$ process is approximately equal to $\Gamma_{K_{1L}(1270)}$. In Figs. 7 (b) and (c), clear peak structures for the $b_1(1235)$ resonance can be observed in the invariant mass distribution of $\omega\pi^+$ and $\phi\pi^+$, respectively.

With Eq. (38), we can calculate the partial decay width of $h_1 \rightarrow K_1^+(1270)K^- \rightarrow K^{*+}\pi^0K^-$ and $h_1 \rightarrow b_1^+(1235)\pi^- \rightarrow b_1^+(1235) \rightarrow \omega(\phi)\pi^+\pi^-$ processes. The theoretical results are shown in Fig. 8 with uncertainties from $\Lambda_t = 1350 \pm 100$ MeV. The partial decay width of $h_1 \rightarrow K_1^+(1270)K^- \rightarrow K^{*+}\pi^0K^-$ is small compared to the $h_1 \rightarrow b_1^+(1235)\pi^- \rightarrow \omega(\phi)\pi^+$ decays, which are in the order of several MeV.

It is known that these partial decay widths are sensitive to the value of the cut-off parameter Λ_t and proportional to the

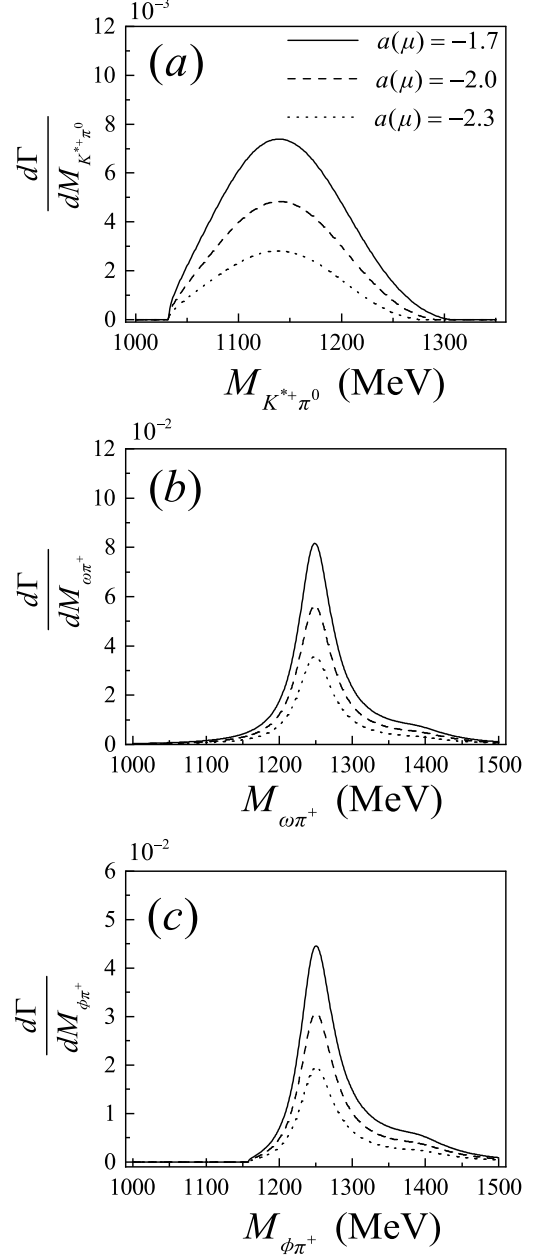


FIG. 7. The invariant mass distribution of (a) $K^{*+}\pi^0$ for $h_1 \rightarrow K_{1L}^+(1270)K^- \rightarrow K^{*+}\pi^0$, (b) $\omega\pi^+$ for $h_1 \rightarrow b_1^+(1235), b_1^+(1235) \rightarrow \omega\pi^+$, and (c) $\phi\pi^+$ for $h_1 \rightarrow b_1^+(1235), b_1^+(1235) \rightarrow \phi\pi^+$ with $a(\mu) = -1.7$ (solid line), -2.0 (dashed line), and -2.3 (dotted line).

product of the coupling constants, which will be cancelled in the ratio between different partial decay widths. Therefore, the ratios among these partial decay widths are interesting, and we define

$$\begin{aligned} R_1 &= \frac{\Gamma_{h_1 \rightarrow K_{1L}\bar{K}, K_{1L} \rightarrow K^*\pi}}{\Gamma_{h_1 \rightarrow b_1\pi, b_1 \rightarrow \omega\pi}}, \\ R_2 &= \frac{\Gamma_{h_1 \rightarrow b_1\pi, b_1 \rightarrow \phi\pi}}{\Gamma_{h_1 \rightarrow b_1\pi, b_1 \rightarrow \omega\pi}}, \end{aligned} \quad (40)$$

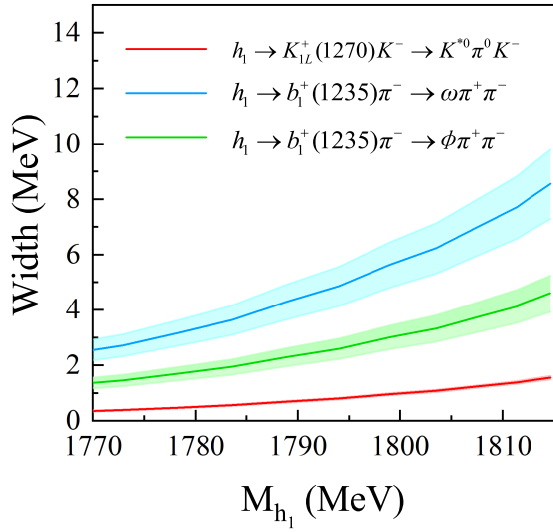


FIG. 8. The partial decay width for the processes $h_1 \rightarrow K_{1L}^+(1270)K^- \rightarrow K^{*+}\pi^0K^-$ (red), $h_1 \rightarrow b_1^+(1235)\pi^- \rightarrow \omega\pi^+\pi^-$ (blue), and $h_1 \rightarrow b_1^+(1235)\pi^- \rightarrow \phi\pi^+\pi^-$ (green) with $\Lambda_t = 1350 \pm 100$ MeV.

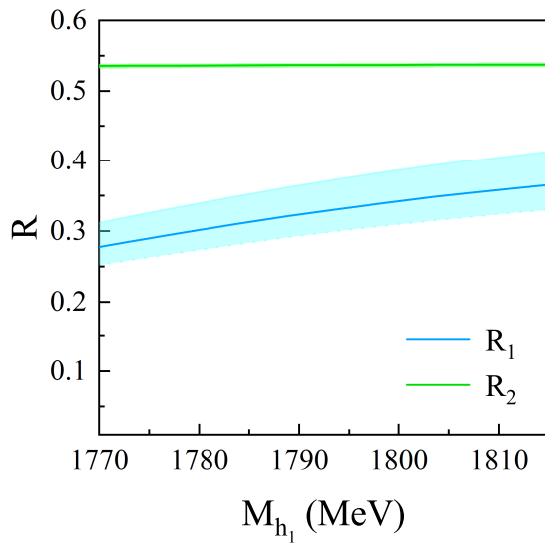


FIG. 9. Theoretical ratios of R_1 (blue) and R_2 (green) for different masses of h_1 with $\Lambda = 1350 \pm 100$ MeV.

where the $K_{1L}(1270)$ and $b_1(1235)$ are written as K_{1L} and b_1 . With the help of isospin symmetry, the ratio of decay widths for the processes $h_1 \rightarrow K_{1L}(1270)\bar{K}$, $K_{1L}(1270) \rightarrow K^*\pi$, $h_1 \rightarrow b_1(1235)\pi$, $b_1(1235) \rightarrow \omega\pi$, and $h_1 \rightarrow b_1(1235)\pi$, $b_1(1235) \rightarrow \phi\pi$ and the widths of the $h_1 \rightarrow K_{1L}^+(1270)K^-$, $K_{1L}^+(1270) \rightarrow K^{*+}\pi^0$, $h_1 \rightarrow b_1^+(1235)\pi^-$, $b_1^+(1235) \rightarrow \omega\pi^+$ and $h_1 \rightarrow b_1^+(1235)\pi^-$, $b_1^+(1235) \rightarrow \phi\pi^+$ are 6, 3, and 3, respectively. The ratios R_1 (blue) and R_2 (green) are shown

in Fig. 9 with $\Lambda = 1350 \pm 100$ MeV. Indeed, they are stable with the mass of M_{h_1} , and R_1 and R_2 are approximately 0.3 and 0.53, respectively.

V. SUMMARY

Hadron spectroscopy offers crucial insights into the non-perturbative regime of quantum chromodynamics. In recent years, the observation of numerous unconventional states such as the XYZ and P_c particles has stimulated intense research into exotic hadrons—including multiquark states, glueballs, and hybrids. A prominent theoretical framework for describing such states is the molecular picture, in which hadrons are understood as bound systems of color-singlet hadrons [1–12]. Within this approach, the ChUT has proven to be an effective tool for studying dynamically generated resonances, leading to many successful predictions and interpretations in hadron spectroscopy [13–41].

In this work, we study the h_1 state dynamically generated from the $K^*\bar{K}^*$ interaction within the ChUT, and examine its decays into $K_1(1270)\bar{K}$ and $b_1(1235)\pi$. The partial widths for $h_1 \rightarrow K_1^+(1270)K^- \rightarrow K^{*+}\pi^0K^-$ and $h_1 \rightarrow b_1^+(1235)\pi^- \rightarrow \omega(\phi)\pi^+\pi^-$ are calculated by including triangle loops involving K^* , \bar{K}^* , and exchanged pseudoscalar mesons. Here, the axial-vector resonances $K_1(1270)$ and $b_1(1235)$ are themselves treated as dynamically generated states from coupled-channel vector–pseudoscalar interactions.

Within the allowed range of model parameters, the partial decay width for $h_1 \rightarrow K_1^+(1270)K^- \rightarrow K^{*+}\pi^0K^-$ is found to be about 0.5 MeV, while those for $h_1 \rightarrow b_1^+(1235)\pi^- \rightarrow \omega(\phi)\pi^+\pi^-$ are of order several MeV. We also present the invariant-mass distributions for $K^{*0}\pi$ from $K_1(1270)$ decay and for $\omega(\phi)\pi$ from $b_1(1235)$ decay. Furthermore, we explore the dependence of the ratios between different decay modes on the mass of the h_1 state—a quantity that could serve as a useful experimental signature. We hope that future experiments will test these predictions, thereby helping to identify the h_1 resonance dynamically generated from $K^*\bar{K}^*$ interactions.

ACKNOWLEDGMENTS

This work is partly supported by the National Key R&D Program of China under Grant No. 2023YFA1606703, and by the National Natural Science Foundation of China under Grant Nos. 12435007, 12361141819, and 1252200936. X.L. is also supported by the National Natural Science Foundation of China under Grant Nos. 12335001 and 12247101, the ‘111 Center’ under Grant No. B20063, the Natural Science Foundation of Gansu Province (No. 22JR5RA389, No. 25JRRRA799), the fundamental Research Funds for the Central Universities, the project for top-notch innovative talents of Gansu province, and Lanzhou City High-Level Talent Funding.

[1] X. Liu, Chin. Sci. Bull. **59**, 3815 (2014), arXiv:1312.7408 [hep-ph].

[2] A. Hosaka, T. Iijima, K. Miyabayashi, Y. Sakai, and S. Yasui, PTEP **2016**, 062C01 (2016), arXiv:1603.09229 [hep-ph].

[3] H.-X. Chen, W. Chen, X. Liu, and S.-L. Zhu, Phys. Rept. **639**, 1 (2016), arXiv:1601.02092 [hep-ph].

[4] R. F. Lebed, R. E. Mitchell, and E. S. Swanson, Prog. Part. Nucl. Phys. **93**, 143 (2017), arXiv:1610.04528 [hep-ph].

[5] F.-K. Guo, C. Hanhart, U.-G. Meißner, Q. Wang, Q. Zhao, and B.-S. Zou, Rev. Mod. Phys. **90**, 015004 (2018), [Erratum: Rev.Mod.Phys. 94, 029901 (2022)], arXiv:1705.00141 [hep-ph].

[6] S. L. Olsen, T. Skwarnicki, and D. Zieminska, Rev. Mod. Phys. **90**, 015003 (2018), arXiv:1708.04012 [hep-ph].

[7] N. Brambilla, S. Eidelman, C. Hanhart, A. Nefediev, C.-P. Shen, C. E. Thomas, A. Vairo, and C.-Z. Yuan, Phys. Rept. **873**, 1 (2020), arXiv:1907.07583 [hep-ex].

[8] J.-M. Richard, Few Body Syst. **57**, 1185 (2016), arXiv:1606.08593 [hep-ph].

[9] L. Meng, B. Wang, G.-J. Wang, and S.-L. Zhu, Phys. Rept. **1019**, 1 (2023), arXiv:2204.08716 [hep-ph].

[10] H.-X. Chen, W. Chen, X. Liu, Y.-R. Liu, and S.-L. Zhu, Rept. Prog. Phys. **86**, 026201 (2023), arXiv:2204.02649 [hep-ph].

[11] M.-Z. Liu, Y.-W. Pan, Z.-W. Liu, T.-W. Wu, J.-X. Lu, and L.-S. Geng, Phys. Rept. **1108**, 1 (2025), arXiv:2404.06399 [hep-ph].

[12] Y.-R. Liu, H.-X. Chen, W. Chen, X. Liu, and S.-L. Zhu, Prog. Part. Nucl. Phys. **107**, 237 (2019), arXiv:1903.11976 [hep-ph].

[13] J. A. Oller and E. Oset, Nucl. Phys. A **620**, 438 (1997), [Erratum: Nucl.Phys.A 652, 407–409 (1999)], arXiv:hep-ph/9702314.

[14] E. Oset and A. Ramos, Nucl. Phys. A **635**, 99 (1998), arXiv:nucl-th/9711022.

[15] J. A. Oller, E. Oset, and J. R. Pelaez, Phys. Rev. D **59**, 074001 (1999), [Erratum: Phys.Rev.D 60, 099906 (1999), Erratum: Phys.Rev.D 75, 099903 (2007)], arXiv:hep-ph/9804209.

[16] T. Inoue, E. Oset, and M. J. Vicente Vacas, Phys. Rev. C **65**, 035204 (2002), arXiv:hep-ph/0110333.

[17] D. Jido, J. A. Oller, E. Oset, A. Ramos, and U. G. Meissner, Nucl. Phys. A **725**, 181 (2003), arXiv:nucl-th/0303062.

[18] L. Roca, E. Oset, and J. Singh, Phys. Rev. D **72**, 014002 (2005), arXiv:hep-ph/0503273.

[19] F.-K. Guo, P.-N. Shen, H.-C. Chiang, R.-G. Ping, and B.-S. Zou, Phys. Lett. B **641**, 278 (2006), arXiv:hep-ph/0603072.

[20] L. Roca, S. Sarkar, V. K. Magas, and E. Oset, Phys. Rev. C **73**, 045208 (2006), arXiv:hep-ph/0603222.

[21] F.-K. Guo, P.-N. Shen, and H.-C. Chiang, Phys. Lett. B **647**, 133 (2007), arXiv:hep-ph/0610008.

[22] L. S. Geng, E. Oset, L. Roca, and J. A. Oller, Phys. Rev. D **75**, 014017 (2007), arXiv:hep-ph/0610217.

[23] D. Gamermann, E. Oset, D. Strottman, and M. J. Vicente Vacas, Phys. Rev. D **76**, 074016 (2007), arXiv:hep-ph/0612179.

[24] D. Gamermann and E. Oset, Eur. Phys. J. A **33**, 119 (2007), arXiv:0704.2314 [hep-ph].

[25] R. Molina, D. Nicmorus, and E. Oset, Phys. Rev. D **78**, 114018 (2008), arXiv:0809.2233 [hep-ph].

[26] L. S. Geng and E. Oset, Phys. Rev. D **79**, 074009 (2009), arXiv:0812.1199 [hep-ph].

[27] S. Sarkar, B.-X. Sun, E. Oset, and M. J. Vicente Vacas, Eur. Phys. J. A **44**, 431 (2010), arXiv:0902.3150 [hep-ph].

[28] C. W. Xiao and E. Oset, Eur. Phys. J. A **49**, 139 (2013), arXiv:1305.0786 [hep-ph].

[29] W. H. Liang, T. Uchino, C. W. Xiao, and E. Oset, Eur. Phys. J. A **51**, 16 (2015), arXiv:1402.5293 [hep-ph].

[30] Y. Zhou, X.-L. Ren, H.-X. Chen, and L.-S. Geng, Phys. Rev. D **90**, 014020 (2014), arXiv:1404.6847 [nucl-th].

[31] J. M. Dias, V. R. Debastiani, J. J. Xie, and E. Oset, Phys. Rev. D **98**, 094017 (2018), arXiv:1805.03286 [hep-ph].

[32] Q.-X. Yu, J. M. Dias, W.-H. Liang, and E. Oset, Eur. Phys. J. C **79**, 1025 (2019), arXiv:1909.13449 [hep-ph].

[33] Z.-Y. Wang and Z.-F. Sun, Eur. Phys. J. C **83**, 1106 (2023), arXiv:2307.00803 [hep-ph].

[34] E. Oset and L. Roca, Eur. Phys. J. C **82**, 882 (2022), [Erratum: Eur.Phys.J.C 82, 1014 (2022)], arXiv:2207.08538 [hep-ph].

[35] Z.-F. Sun, J.-J. Xie, and E. Oset, Phys. Rev. D **97**, 094031 (2018), arXiv:1801.04367 [hep-ph].

[36] S. Sakai, L. Roca, and E. Oset, Phys. Rev. D **96**, 054023 (2017), arXiv:1704.02196 [hep-ph].

[37] J. M. Dias, F. Aceti, and E. Oset, Phys. Rev. D **91**, 076001 (2015), arXiv:1410.1785 [hep-ph].

[38] R. Molina, T. Branz, and E. Oset, Phys. Rev. D **82**, 014010 (2010), arXiv:1005.0335 [hep-ph].

[39] R. Molina and E. Oset, Phys. Rev. D **80**, 114013 (2009), arXiv:0907.3043 [hep-ph].

[40] E. Oset, A. Ramos, and C. Bennhold, Phys. Lett. B **527**, 99 (2002), [Erratum: Phys.Lett.B 530, 260–260 (2002)], arXiv:nucl-th/0109006.

[41] S. Sarkar, E. Oset, and M. J. Vicente Vacas, Nucl. Phys. A **750**, 294 (2005), [Erratum: Nucl.Phys.A 780, 90–90 (2006)], arXiv:nucl-th/0407025.

[42] M. Ablikim *et al.* (BES), Phys. Lett. B **685**, 27 (2010), arXiv:0909.2087 [hep-ex].

[43] J.-J. Xie, M. Albaladejo, and E. Oset, Phys. Lett. B **728**, 319 (2014), arXiv:1306.6594 [hep-ph].

[44] X.-L. Ren, L.-S. Geng, E. Oset, and J. Meng, Eur. Phys. J. A **50**, 133 (2014), arXiv:1405.0153 [nucl-th].

[45] H. Nagahiro, L. Roca, A. Hosaka, and E. Oset, Phys. Rev. D **79**, 014015 (2009), arXiv:0809.0943 [hep-ph].

[46] J.-M. Xie, J.-X. Lu, L.-S. Geng, and B.-S. Zou, Phys. Rev. D **108**, L111502 (2023), arXiv:2307.11631 [hep-ph].

[47] J.-M. Xie, Z.-W. Liu, J.-X. Lu, H. Liang, R. Molina, and L.-S. Geng, (2025), arXiv:2511.14380 [hep-ph].

[48] L. Roca, A. Hosaka, and E. Oset, Phys. Lett. B **658**, 17 (2007), arXiv:hep-ph/0611075.

[49] F. Aceti, J. M. Dias, and E. Oset, Eur. Phys. J. A **51**, 48 (2015), arXiv:1501.06505 [hep-ph].

[50] F. Aceti, J.-J. Xie, and E. Oset, Phys. Lett. B **750**, 609 (2015), arXiv:1505.06134 [hep-ph].

[51] J.-J. Xie, Phys. Rev. C **92**, 065203 (2015), arXiv:1509.06196 [nucl-th].

[52] R. Molina, M. Doering, W. H. Liang, and E. Oset, Eur. Phys. J. C **81**, 782 (2021), arXiv:2107.07439 [hep-ph].

[53] Q.-H. Shen, L.-S. Geng, and J.-J. Xie, Eur. Phys. J. A **61**, 42 (2025), arXiv:2409.05302 [hep-ph].

[54] D. Gülmез, U. G. Meißner, and J. A. Oller, Eur. Phys. J. C **77**, 460 (2017), arXiv:1611.00168 [hep-ph].

[55] Z.-L. Wang and B.-S. Zou, Phys. Rev. D **104**, 114001 (2021), arXiv:2107.14470 [hep-ph].

[56] Z.-L. Wang and B.-S. Zou, Eur. Phys. J. C **82**, 509 (2022), arXiv:2203.02899 [hep-ph].

[57] A. I. Titov, B. Kampfer, and B. L. Reznik, Eur. Phys. J. A **7**, 543 (2000), arXiv:nucl-th/0001027.

[58] A. I. Titov, B. Kampfer, and B. L. Reznik, Phys. Rev. C **65**,

065202 (2002), arXiv:nucl-th/0102032.

[59] L. R. Dai, L. Roca, and E. Oset, Eur. Phys. J. C **80**, 673 (2020), arXiv:2005.02653 [hep-ph].

[60] P.-L. Lü and J. He, Eur. Phys. J. A **52**, 359 (2016), arXiv:1603.04168 [hep-ph].

[61] L. R. Dai, L. Roca, and E. Oset, Phys. Rev. D **99**, 096003 (2019), arXiv:1811.06875 [hep-ph].

[62] C.-H. Zeng, J.-X. Lu, E. Wang, J.-J. Xie, and L.-S. Geng, Phys. Rev. D **102**, 076009 (2020), arXiv:2006.15547 [hep-ph].